Remote Sensing of Environment 112 (2008) 4344–4357

Contents lists available at ScienceDirect

Remote Sensing of Environment

journal homepage: www.elsevier.com/locate/rse

A lidar-based hierarchical approach for assessing MODIS fPAR

L. Chasmer [a,*], C. Hopkinson [b], P. Treitz [a], H. McCaughey [a], A. Barr [c], A. Black [d]

[a] Department of Geography, Queen's University, Kingston ON, Canada K7L 3N6
[b] Applied Geomatics Research Group, Lawrencetown NS, Canada B0S 1M0
[c] Climate Research Branch, Meteorological Service of Canada, Saskatoon SK, Canada S7N 3H5
[d] Faculty of Land and Food Systems, University of British Columbia, Vancouver BC, Canada V6T 1Z4

ARTICLE INFO

Article history:
Received 14 April 2008
Received in revised form 1 August 2008
Accepted 2 August 2008

Keywords:
Airborne lidar
MODIS
fPAR
LAI
Scaling
Boreal forest

ABSTRACT

The purpose of this study was to estimate the fraction of photosynthetically active radiation absorbed by the canopy (fPAR) from point measurements to airborne lidar for hierarchical scaling up and assessment of the Moderate Resolution Imaging Spectroradiometer (MODIS) fPAR product within a "medium-sized" (7 km×18 km) watershed. Nine sites across Canada, containing one or more (of 11) distinct species types and age classes at varying stages of regeneration and seasonal phenology were examined using a combination of discrete pulse airborne scanning Light Detection And Ranging (lidar) and coincident analog and digital hemispherical photography (HP). Estimates of fPAR were first compared using three methods: PAR radiation sensors, HP, and airborne lidar. HP provided reasonable estimates of fPAR when compared with radiation sensors. A simplified fractional canopy cover ratio from lidar based on the number of within canopy returns to the total number of returns was then compared with fPAR estimated from HP at 486 geographically registered measurement locations. The return ratio fractional cover method from lidar compared well with HP-derived fPAR (coefficient of determination=0.72, RMSE=0.11), despite varying the lidar survey configurations, canopy structural characteristics, seasonal phenologies, and possible slight inaccuracies in location using handheld GPS at some sites. Lidar-derived fractional cover estimates of fPAR were ~10% larger than those obtained using HP (after removing wood components), indicating that lidar likely provides a more realistic estimate of fPAR than HP when compared with radiation sensors. Finally, fPAR derived from lidar fractional cover was modelled at 1 m resolution and averaged over 99 1 km areas for comparison with MODIS fPAR. The following study is one of the first to scale between plot measurements and MODIS pixels using airborne lidar.

1. Introduction

Covering approximately 76% of the global land surface area, vegetation plays a key role in the functioning of local ecosystems and can affect processes at scales as large as global weather patterns (Pielke et al., 1998). Leaf area is particularly important, affecting energy and mass exchanges between the terrestrial biosphere and the atmosphere (e.g. Chen et al., 2005). Accurate spatial and temporal estimates of measurable leaf attributes: leaf area index (LAI) and the fraction of photosynthetically active radiation absorbed by the canopy (fPAR), are required as inputs into models of plant production and exchange of heat, water vapour, and CO_2 with the atmosphere (e.g. Chen et al., 2007; Gower et al., 1999). The accuracy of many models, therefore, depends on accurate inputs of these key variables.

Chen et al. (2002) defines LAI as the upper part of the total leaf surface area of all leaves contained within a unit of ground surface area ($m^2\ m^{-2}$). This definition of LAI is most appropriate in the context of energy and CO_2/H_2O mass balance because it only includes the actively photosynthesizing parts of the canopy and is important for global photosynthesis (e.g. gross primary production) modeling using remote sensing. fPAR can be estimated from radiation sensors based on the ratio:

$$\mathrm{fPAR} = \left((\mathrm{PAR}_{\mathrm{AC}\downarrow} - PAR_{\mathrm{AC}\uparrow}) - (PAR_{\mathrm{BC}\downarrow} - PAR_{\mathrm{BC}\uparrow})\right)/\mathrm{PAR}_{\mathrm{AC}\downarrow} \quad (1)$$

where $\mathrm{PAR}_{\mathrm{AC}\downarrow}$ is the incident PAR above the canopy, $\mathrm{PAR}_{\mathrm{AC}\uparrow}$ is the reflected PAR above the canopy, $\mathrm{PAR}_{\mathrm{BC}\downarrow}$ is the incident below-canopy PAR after interception by branches and leaves, and $\mathrm{PAR}_{\mathrm{BC}\uparrow}$ is the reflected PAR from the ground surface after absorption by soils (Gower et al., 1999). The MODIS fPAR algorithm, however, excludes PAR absorbed by the soil (via soil albedo) and only considers PAR absorbed by vegetation. Despite their importance, LAI and fPAR are difficult and time consuming to measure spatially and temporally within ecosystems. Both require measurement of canopy fractional cover (or canopy closure) and light transmission (optical methods), or alternative approaches involving destructive sampling of leaves and branches. Optical methods are less time consuming than destructive sampling, and are more frequently used (Jonckheere et al., 2004). These rely on

* Corresponding author.
E-mail address: lechasme@yahoo.ca (L. Chasmer).

0034-4257/$ – see front matter © 2008 Elsevier Inc. All rights reserved.
doi:10.1016/j.rse.2008.08.003

temporal measurements from radiation sensors located above and below the canopy on a meteorological tower (e.g. Gower et al., 1999; Huemmrich et al., 1999; Schwalm et al., 2006; Eq. (1)). They can also be collected spatially below the canopy via incident hemispherical radiation measurement units such as the LiCOR LI-2000 Plant Canopy Analyzer, TRAC, and hemispherical photography (HP) (e.g. Chen et al., 2006; Leblanc et al., 2005; Sonnentag et al., 2007). Measurements from radiation sensors on towers are beneficial because they record phenological changes in vegetation over seasons, but are affected by changes in solar zenith angles (Hyer & Goetz, 2004). Hemispherical radiation measurements can also be operated as handheld devices by field personnel, and can be used at a variety of plots (Leblanc et al., 2005) or transects (Chen et al., 2006) within a larger study area. They are inexpensive to operate, but remote study locations often make it difficult to measure changes frequently throughout the growing season (Heinsch et al., 2006). Some comparisons have been made between different optical methods. For example, Chen et al. (2006) found that HP tended to slightly underestimate effective LAI (L_e) by approximately 8%, on average for a number of forest types when compared with the LiCOR LI-2000 method. L_e is related canopy gap fraction estimated using optical methods and assumes that foliage is randomly distributed within the canopy. It therefore does not include the effects of canopy clumping and may be more associated with projected leaf area viewed using remote sensing methods (Chen et al., 2004). Chen et al. (2006) note that the overall HP estimates of L_e agree very well with those estimated using the LI-2000 at a number of forest sites examined within the Canadian Carbon Program.

Other methods used to estimate LAI and fPAR include measurements of reflected light collected using remote sensing satellite and airborne platforms (Gamon et al., 2004), for example the Moderate Resolution Imaging Spectroradiometer (MODIS). Remote sensing methods using spectral reflectance alone, however, are not able to resolve the complexity of the vegetation canopy within averaged pixels of fPAR and LAI (e.g. Eriksson et al., 2006; Jin et al., 2007; Xu et al., 2004). Radiative transfer models often improve spectral reflectance measurements by incorporating species-based three-dimensional canopy structure, leaf and stem geometry, and foliage density at the tree to canopy level (e.g. Fernandes et al., 2004; Goel & Thompson, 2000; Myneni et al., 1997; Sun & Ranson, 2000). These can be directly related to variability in canopy reflectance measured using remote sensing methods. However, canopy heterogeneity within species and at different layers within the canopy can lead to uncertainties in radiative transfer models (Kotchenova et al., 2004; Tian et al., 2002a,b), and the possibility of numerous results per species type (e.g. Koetz et al., 2006). Accurate spatial and temporal methods of collecting fPAR and LAI would be beneficial and cost-effective for scaling from radiation sensors to wider area coverage. Canopy structural attributes may also be used to better interpret averaged spectral signatures within lower spectral resolution pixels (Koetz et al., 2006; Kotchenova et al., 2004).

The fractional cover of vegetation (used synonymously with full hemisphere fractional canopy closure in this study), where 1=full canopy cover and 0=no canopy cover may also be estimated from airborne Light Detection and Ranging (lidar). Fractional cover from lidar may be converted into LAI and fPAR based on the ratio of the number of canopy laser returns (single and multiple) to total returns (e.g. Barilotti et al., 2006; Hopkinson & Chasmer, 2007; Magnussen & Boudewyn, 1998; Morsdorf et al., 2006; Riaño et al., 2004; Solberg et al., 2006; Todd et al., 2003):

$$f\text{cover} = \left(\frac{\sum P_{\text{canopy}}}{\sum P_{\text{all}}}\right). \quad (2)$$

P_{canopy} is the total number of laser pulse returns within the canopy, and P_{all} is the total number of all laser pulse returns within a specified resolution (e.g. 1 m). Depending on the lidar system used, multiple laser returns will be recorded from within the canopy and understory at heights greater than ~1.5 m above the ground surface (Hopkinson et al., 2005), but only single returns will be recorded at heights less than ~1.5 m. Solberg et al. (2006) apply a slightly modified version of Eq. (2) by including a radiation extinction coefficient. Morsdorf et al. (2006) examine numerous laser pulse ratios and HP annulus ring configurations, and found that central rings combined with first pulse returns provide the same correlation as when using first and last returns, when compared with field estimates. However, first returns tended to yield greater *f*cover than field estimates, whereas last returns tended to yield estimates that were less than those found in the field. Also, the extraction of lidar data within a circular area mimicked by HP ("data traps", Lovell et al., 2003; Morsdorf et al., 2006) were found to be most appropriate when radii of up to 2 m were used (Morsdorf et al., 2006). Riaño et al. (2004) related lidar data traps to the height of the tree, and found that this provided the best results when correlating fractional cover to LAI or fPAR. In Hopkinson and Chasmer (2007), the use of annulus rings 1 and 2 provided noisy results because of locally varying canopy gaps and the inability to accurately geo-register HP to lidar using GPS methods at this scale. They, therefore, opted for a larger data trap of 11.3 m radius and included annulus rings 1–9. The *f*cover ratio in Eq. (2) may estimate a slightly greater fractional cover when compared with results from HP based on annulus rings used, scan angle influences, and the use of first and single returns vs. multiple returns but tends to be within about 20% of HP (e.g. Hopkinson & Chasmer, 2007; Morsdorf et al., 2006). Hopkinson and Chasmer (2007) use laser pulse intensity as an indicator of transmission losses through the canopy. They found that the intensity-based approach provided slightly better estimates of gap fraction than the commonly used ratio in Eq. (2), but more importantly, did not require calibration (e.g. had a 1:1 relationship, regardless of seasonal cycle and sensor configuration).

Current studies that use lidar to estimate LAI, L_e, fractional cover (at nadir) or canopy cover (entire hemisphere), gap fraction, and fPAR tend to concentrate on one or a few different forest types within a specified location (e.g. Thomas et al., 2006) and often with controlled lidar survey configurations (e.g. Hopkinson & Chasmer, 2007). It is not clear if the return ratio method can be applied universally to a range of forest vegetation species types and structural characteristics. If the model is universally applicable (i.e. with little error), then it may be used as a simple methodology for assessing MODIS fPAR and LAI products in combination with point estimates from HP. This study presents results from a cross-Canada transect of lidar and HP data. The return ratio method (2) is especially relevant for cases where normalized (i.e. geometrically corrected) laser return intensity information may not be available (e.g. Hopkinson & Chasmer, 2007, in review). Three objectives will be examined:

1. Compare fPAR estimated using radiation sensors and fPAR estimated using HP methods. If fPAR estimated using HP compares well with fPAR estimated using radiation sensors, then we assume that fPAR from HP provides a good approximation of fPAR from radiation sensors, and can be applied spatially.
2. fPAR from HP at 486 geo-registered photo plots across Canada are compared with the lidar fractional canopy cover return ratio (*f*cover) (2).
3. Comparisons are then made between 99 1 km resolution MODIS pixels of fPAR and pixel-average lidar fPAR within a medium-sized watershed.

Airborne lidar may provide a useful alternative for mapping fPAR at high resolutions, especially in areas where mixed pixels and understory contribute to average reflectance characteristics of lower spectral resolution remote sensing products (e.g. MODIS) (Serbin et al., in press). Relationships between mixed pixels, land cover type, and canopy structural characteristics found in lidar data may be used to better understand inconsistencies in MODIS fPAR/LAI products

without the need for extensive field validation. Inexpensive and sometimes free lidar data are available through a number of website and contact listings (e.g. the United States Geological Survey CLICK program), providing users with access to already available lidar datasets within vegetated environments. This study presents on the hierarchical scaling of point measurements to larger landscape areas using radiation sensors, plot measurements, high resolution lidar, and low resolution MODIS pixels of fPAR. If successful, a simple lidar methodology for estimating fPAR could be an important step towards improving ecosystem models and also validating remote sensing products, such as those from MODIS.

2. Study areas

The study was conducted over 9 sites, along east to west and north to south Canadian transects between the years 2002 and 2007 (Fig. 1), with coincident HP. Each site contains one to many different forest species types, varying ages, and canopy structural characteristics (Table 1). In many cases, the same species were found at a number of different sites, providing statistical confidence and reproducibility of the experiment in different areas. Sites also vary in topography, where some sites are flat (e.g. Annapolis Valley and York Region), other sites are gently rolling (e.g. Lac Duparquet and Lake Utikama), whilst still other sites are mountainous with steep terrain (e.g. Bow Summit and Wolf Creek). It is not currently known if topography will influence the lidar canopy cover; however, inclusion of sites from a wide variety of terrain types will provide some indication of possible errors, if they exist, as a result of slope angle. Site characteristics and locations are provided in Table 1 and Fig. 2. Two sites, the Annapolis Valley forest and York Regional forest have been surveyed using airborne lidar and HP multiple times throughout the growing seasons between 2000 and 2007 for continuing studies on phenology and growth (e.g. Hopkinson & Chasmer, 2007; Hopkinson et al., 2008). The White Gull River watershed, which contains the BERMS jack pine chronosequence, Saskatchewan, has been used for MODIS fPAR assessment. This watershed contains a mixture of southern boreal forest vegetation classes and disturbance regimes, providing an ideal test of both airborne lidar methods and the MODIS fPAR product.

3. Methodology

3.1. HP data collection and analysis

Canopy gap fraction was collected using HP at geo-located sites within representative forest types throughout each study area (Fig. 2). Photographic plots were set up in two ways: a) as individual plots containing five photographs. One photograph was taken at the centre of the plot, and four were located 11.3 m from the centre along cardinal (N, S, E, and W) directions, determined using a compass bearing and measuring tape following Fluxnet-Canada and the Canadian Carbon Program protocol (Fluxnet-Canada, 2003); and b) along transects of varying lengths and distances between photos. Photographs that were taken within photo plots (a) were located at the centre of the plot using survey-grade, differentially corrected global positioning system (GPS) receivers (Leica SR530, Leica Geosystems Inc. Switzerland; Ashtec Locus, Ashtec Inc., Hicksville, NY) with the same base station coordinate as was used for the lidar surveys. Geolocation accuracies varied from 1 cm to 1 m depending on the canopy cover density at the time of GPS data collection. Measuring tape and compass bearing methods were then used to locate cardinal photographs to approximately 1 m to 2 m accuracy. Photographs that were taken along transects (b) were located using WAAS-enabled (wide area augmentation service) handheld GPS (Trimble Inc. GeoExplorer, Idaho, USA). These photographs have a locational

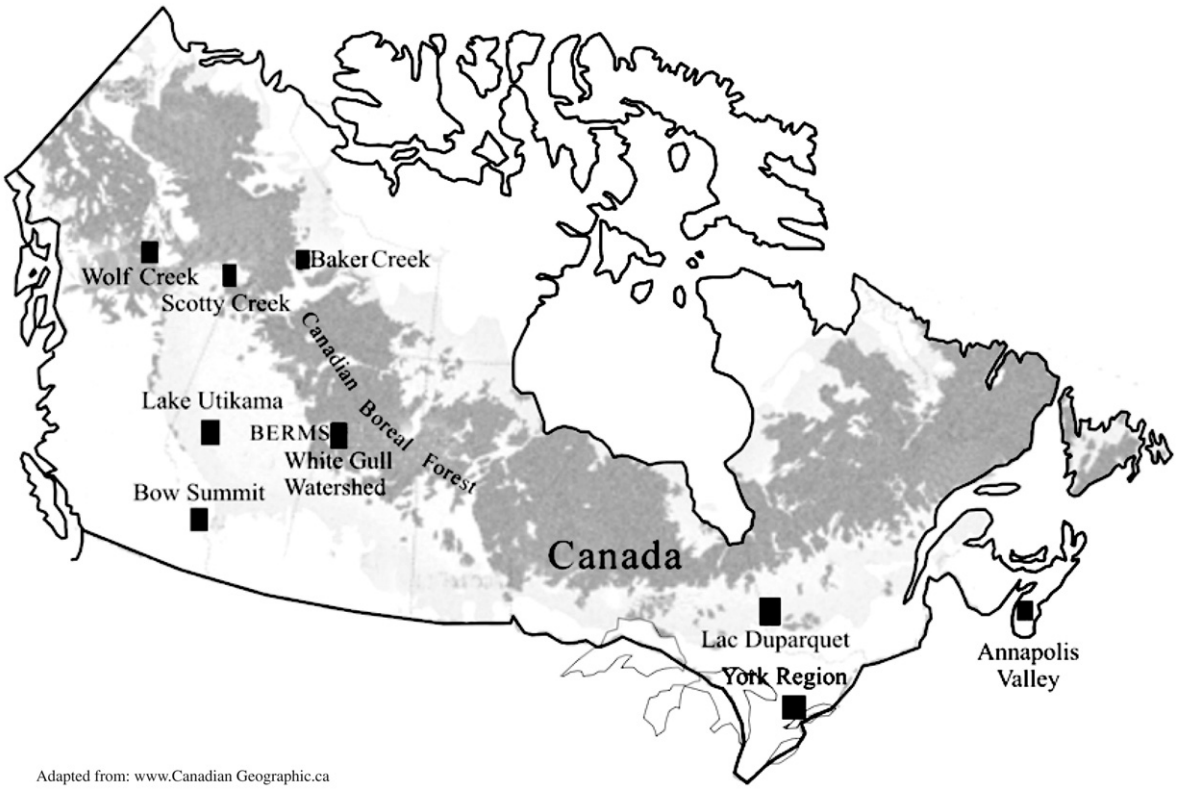

Fig. 1. Map of the lidar surveys and areas studied. The dark grey area represents the extent and location of the Canadian boreal forest, whereas light grey areas represent southern temperate forests and the northern forest-tundra transition. BERMS jack pine sites are found within the larger White Gull River watershed (surveyed at the same time with the same lidar configuration).

Table 1
Forest HP plot descriptions and species type per site location

Site (dominant canopy species)	Code[a]	Location	~ Latitude, Longitude (Deg. Min.)	Age (yrs)	Average Height (m)	Average LAI	Reference(s) on Sites and Methods
Mature red pine (*Pinus resinosa* Ait.)	MRP-ON	York Regional Forest, Newmarket Ontario (ON)	44.0772808 −79.323299	50	23	4.2	Hopkinson et al. (2008); Chasmer et al. (2006); Hopkinson et al. (2004)
Mature hardwood (*Acer saccharum* Marsh.; *Quercus rubra* L. *Betulla alleghaniensis* Britt.)	MHW-ON	York Regional Forest, Newmarket ON	44.0772808 −79.323299	75	19	2.9	Chasmer et al. (2006); Hopkinson et al. (2004)
Mature sub-alpine fir (*Abies lasiocarpa* Nutt.)	MSAF-AB	Bow Summit, Banff National Park, Alberta (AB)	51.7161044 −116.49289	40	9	0.9	Hopkinson and Demuth (2006)
Mature trembling aspen (*Populus tremuloides* Michx.)	MTA-AB	Lake Utikama, AB	56.1094298 −115.65553	–	16	0.8	Hopkinson et al. (2005); Hopkinson et al. (2006)
Mature black spruce (*Picea mariana* Mill.)	MBS-AB	Lake Utikama, AB	56.1041838 −115.64003	–	7	0.6	Hopkinson et al. (2005); Hopkinson et al. (2006)
Old jack pine (*Pinus banksiana* Lamb.)	OJP-SK	Prince Albert National Park, Saskatchewan (SK)	53.9173320 −104.69168	90	14	1.6	Chen et al. (2006); Schwalm et al. (2006)
Harvested 1975 jack pine (*Pinus banksiana* Lamb.)	HJP75-SK	Prince Albert National Park, SK	53.8765147 −104.64487	30	6.3	2.8	Chen et al. (2006); Schwalm et al. (2006)
Harvested 1994 jack pine (*Pinus banksiana* Lamb.)	HJP94-SK	Prince Albert National Park, SK	53.908632 −104.65728	11	1.6	1.1	Chen et al. (2006); Schwalm et al. (2006)
Mature acadian mixed-wood (*Acer saccharum* Marsh., *Pinus strobus* L. *Betula alleghaniensis* Britt.)	MAMW-NS	Annapolis Valley, Nova Scotia (NS)	44.9123464 −65.076174	100	21	3.4	Hopkinson and Chasmer (2007)
Immature birch (*Betula alleghaniensis* Britt.)	IB-NS	Annapolis Valley, NS	44.9129791 −65.075440	12	5	2.5	Hopkinson and Chasmer (2007)
Mature hardwood (*Acer saccharum* Marsh.; *Quercus rubra* L.)	MHW-NS	Annapolis Valley, NS	44.9200606 −65.078282	70	22	2.9	Hopkinson and Chasmer (2007)
Mature trembling aspen (*Populus tremuloides* Michx.)	MTA-QC	Lac Duparquet, Quebec (QC)	48.4604999 −79.438000	–	26	1.7	St Onge and Vepakomma (2004)
Mature birch (*Betula alleghaniensis* Britt.)	MB-QC	Lac Duparquet, QC	48.4644999 −79.436666	–	20	1.7	St Onge and Vepakomma (2004)
Mature jack pine (*Pinus banksiana* Lamb.)	MJP-QC	Lac Duparquet, QC	48.4601666 −79.438000	–	23	2.8	St Onge and Vepakomma (2004)
Mature white spruce (*Picea glauca* (Moench) Voss.)	MWS-YT	Wolf Creek, Whitehorse, Yukon Territories (YT)	60.6050500 −135.03460	–	10	0.2 (effective LAI)	Pomeroy et al. (2005); Quinton et al. (2005)
Mixed trembling aspen and black spruce (*Populus tremuloides* Michx. *Picea mariana* Mill.)	MABS-NWT	Scotty Creek, Fort Simpson, Northwest Territories (NWT)	61.4408000 −121.25435	–	20	1.2 (effective LAI)	Hayashi et al. (2007)
Mature trembling aspen (*Populus tremuloides* Michx.)	MTA-NWT	Baker Creek, Yellowknife NWT	62.5421015 −108.37179	–	7	1.23	–
Mature black spruce (*Picea mariana* Mill.)	NBS-NWT	Baker Creek, Yellowknife NWT	62.5366244 −108.36805	–	9	0.18	–
Mature birch (*Betula alleghaniensis* Britt.)	MB-NWT	Baker Creek, Yellowknife NWT	62.5422871 −108.37115	–	5	2.31	–

– Represent unavailable data.
[a] Code conventions follow: 1st letter, age (I = immature, or M = mature) or stand type (H = harvested); 2nd, 3rd, and 4th letters, dominant stand type (e.g. BS = black spruce, AMW = Acadian mixed-wood) and last two to three letters = province or territory.

accuracy of between 2 m and 10 m depending on GPS satellite configuration and canopy cover at the time of data collection. Those sites that were revisited more than once using HP (e.g. Annapolis Valley) had permanent stakes of photo locations, for repeatability of photographs. Photographs at all sites except for the HJP94-SK site were taken at a height of ~1.3 m, whereas HJP94-SK was taken at a height of 0.7 m. This was due to the height of trees within this regenerating stand being often less than 2 m in height. The heights of the photographs (taken above the ground surface) were also used to extract within canopy lidar returns. All photographs were taken during either diffuse daytime conditions, or 30 min before dawn or after dusk to reduce the influence of sun brightness and apparent leaf reduction within the photograph (Zhang et al., 2005). Photographs were also under-exposed by one f-stop below automatic exposure (normally set between one and four exposure settings and with larger aperture) (Chen et al., 2006).

Each individual photograph was processed following sky and vegetation thresholding methods of Leblanc et al. (2005) to obtain estimates of gap fraction (Ω) and effective leaf area (L_e). Analog photos were digitized at high resolution (4 megapixels) within a photography and camera store (Henry's, Kingston Ontario) prior to analysis. DHP version 1.6.1 software was used to process all photographs (S. Leblanc, Canada Centre for Remote Sensing provided to L. Chasmer through the Fluxnet-Canada Research Network). Table 2 summarises the dates of the survey and types of cameras and lenses used. All photographs were collected coincident to or within a few days of the lidar survey to avoid seasonal changes in vegetation.

Estimates of fPAR were determined from HP based on L_e from annulus rings 1–5 (0–45°) and 1–9 (0–81°) from individual photographs, following the methodology presented Gower et al. (1999) and modified to include albedo in Chen et al. (2006):

$$f\mathrm{PAR} = (1-\rho_a)-(1-\rho_u)e^{-0.45(1-\alpha)L_e/\cos\theta} \quad (3)$$

where α is wood fraction, ρ_a is the PAR albedo of the stand (i.e., above canopy), ρ_u is the PAR albedo of the ground, and θ is the solar zenith angle at 12:00 local standard time (LST) on the date of the lidar survey, which was within one or two days of the HP collection. Local solar time is used so that comparisons can be made with estimates from Chen et al. (2006) for the same sites. Chen et al. (2006) also use solar noon in their calculations of fPAR to avoid seasonal and diurnal variability due to solar zenith angles. Chen et al. (2006) suggest using a constant extinction coefficient of 0.45 in the calculation of fPAR to account for multiple scattering within the canopy. They also suggest multiplying L_e by a scaling factor of 1.16 using LI-2000 and HP methods (Chen et al., 2006) prior to calculation of fPAR in Eq. (3) because the multiple scattering of light within the canopy causes a negative bias of 16%, on average when rings 1–3 vs. rings 1–5 are used. This bias also tends to increase at larger zenith angles (Chen et al., 2006). Examination of the multiple scattering effect and possible

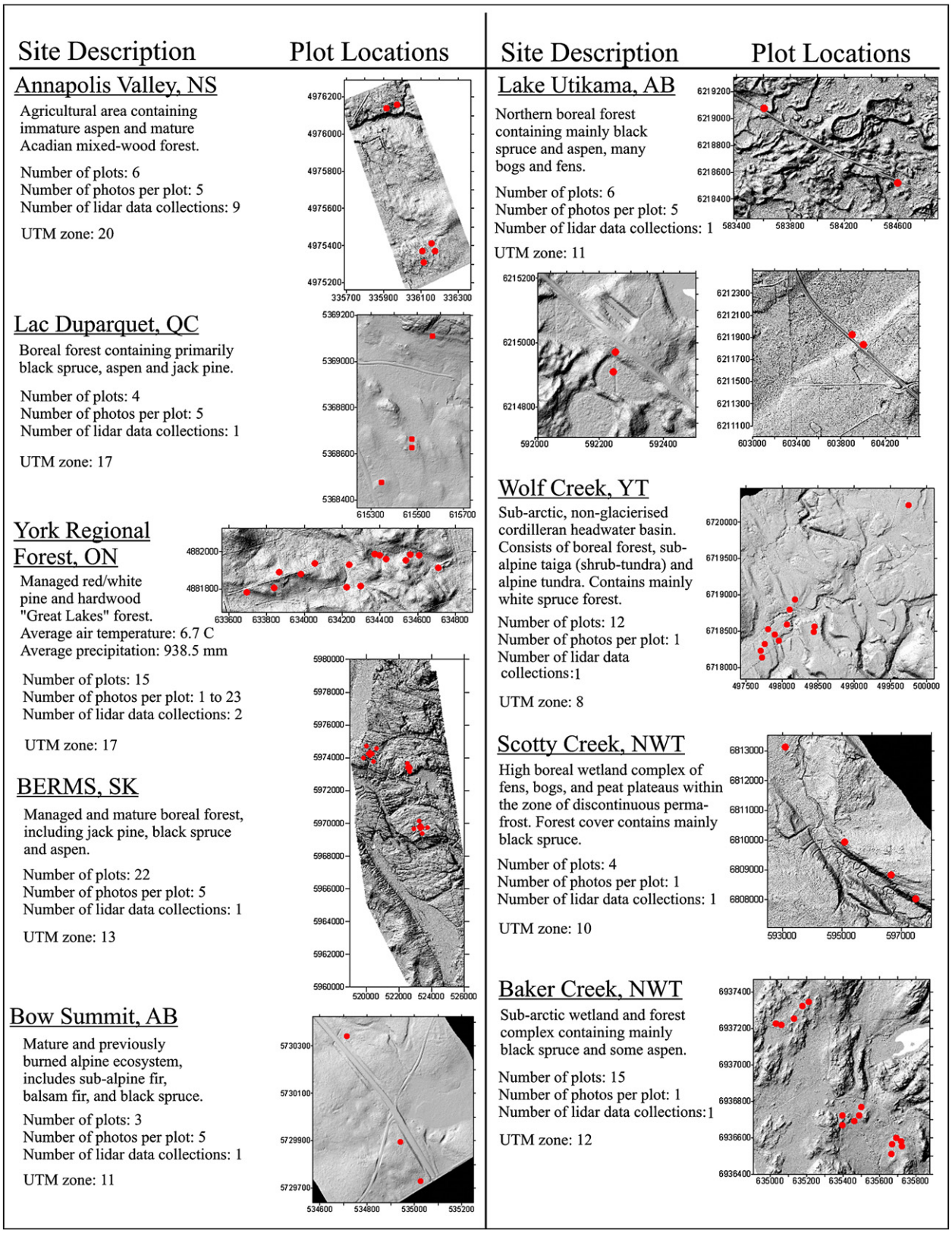

Fig. 2. Description of individual lidar survey sites. Red circles represent HP plot locations and areas where lidar data are extracted on a plot by plot basis. The shaded relief digital elevation models (DEMs) have been created using an inverse-distance weighting procedure of varying resolutions (1 m to 5 m, depending on laser return spot spacing) based on lidar ground returns only. Universal Transverse Mercator (UTM) (NAD83) coordinates are provided on *x* and *y* axes of each DEM and indicate scale (m).

biases is beyond the scope of the present study, and therefore, we have elected to use the average ratio provided in Chen et al. (2006). When making comparisons between HP and lidar, wood fraction (α) was included in Eq. (3), resulting in an analysis of green fPAR only (i.e. reduction of fPAR based on allometric estimates of wood fraction). We examined green fPAR because HP preferentially views more woody

Table 2
HP set up and geo-location at individual plots within larger site areas

Survey site location (containing up to many species types)	Date(s) of photo survey	Camera model used	Lens type	Height of photo (m)	Time of day	# of photo per plot	Coordinate location device	Approx. photo accuracy: within (m) of 11.3 m lidar plot location
York Regional Forest, ON	July 8, 2002 July 9, 2007	Nikon F-601 AF Nikon Coolpix 8.0 mega pixel	Nikkor 8 mm 180° fisheye lens Nikon FC-E9 180° fisheye converter	1.3	dusk	20	Survey GPS of corners, tape and bearing to photo centres	<4
Bow Summit, AB	August 22, 2002	Nikon F-601 AF	Nikkor 8 mm 180° fisheye lens	1.3	Midday diffuse	5	Survey GPS of corners, tape and bearing to photo centres	<4
Lake Utikama, AB	August 25–30 2002	Nikon F-601 AF	Nikkor 8 mm 180° fisheye lens	1.3	Midday diffuse	5	Survey GPS of corners, tape and bearing to photo centres	<4
BERMS, SK	August 10–20, 2005	Nikon Coolpix 8.0 mega pixel	Nikon FC-E9 180° fisheye converter	1.3 (0.7 m at HJP94)	30 min before dusk/after dawn	5	Survey GPS of centre of photo plot, tape and bearing 11.3 m to N, S, E, and W centre photos	<1
Annapolis Valley, NS	April 8, 2006, May 12, 2006, May 27, 2006, Aug. 18, 2006, Oct. 8, 2006, July 24, 2007, Sept. 24, 2007, Dec. 3, 2007	Nikon Coolpix 8.0 mega pixel	Nikon FC-E9 180° fisheye converter	1.3	Midday diffuse and dusk/dawn	5	Survey GPS of centre of photo plot, tape and bearing 11.3 m to N,S,E, and W centre photos	<1
Lac Duparquet, QC	July 11, 2007	Nikon Coolpix 8.0 mega pixel	Nikon FC-E9 180° fisheye converter	1.3	Midday diffuse	5	Handheld GPS of centre of photo plot, tape and bearing 11.3 m to N,S,E, and W centre photos	Between 2 m and 10 m
Wolf Creek, YT	Aug. 12, 2007	Nikon Coolpix 8.0 mega pixel	Nikon FC-E9 180° fisheye converter	1.3	Midday diffuse	1	Handheld GPS of centre of single photo	Between 2 m and 10 m
Scotty Creek, NWT	Aug. 15, 2007	Nikon Coolpix 8.0 mega pixel	Nikon FC-E9 180° fisheye converter	1.3	Midday diffuse	1	Handheld GPS of centre of single photo	Between 2 m and 10 m
Baker Creek, NWT	Aug. 20, 2007	Nikon Coolpix 8.0 mega pixel	Nikon FC-E9 180° fisheye converter	1.3	Midday diffuse	1	Handheld GPS of centre of single photo	Between 2 m and 10 m

components (stems and branches) than lidar because of its location beneath the canopy and the field of view of the camera lens. Lidar, however, scans vegetation from hundreds of meters above the canopy, and therefore the probability of returns from leaves within the canopy is likely greater than from stems and branches. Therefore it was assumed that returns from wood components within the lidar data were negligible. Wood fraction and albedo were determined from the literature (presented in Table 6).

3.2. Validation of HP using PAR sensors

The fraction of PAR absorbed, derived from HP, was validated using Eq. (1) at five sites where measurements of PAR have been made above and below the canopy (at the approximate height of HP). These sites include: BERMS (Saskatchewan) OJP-SK, HJP75-SK, and Annapolis Valley (Nova Scotia) MAMW-NS, IB-NS, and MHW-NS. At BERMS, towers were located at the centre of the sites and between photo plots (located 100 and 500 m from the tower). Therefore location-specific and varying canopy heterogeneity within HP plots was not captured by PAR sensors at the Saskatchewan sites, but do provide a general estimate of fPAR if we can assume that the canopy is fairly homogeneous. In the case of the NS sites, radiation measurements were made within 1 m of HP estimates (specific to the location of the tower, and not including separate plot measurements) and were therefore representative of the canopy viewed by HP and airborne lidar.

Above- and below-canopy radiation measurements of PAR (μmol m^{-2} s^{-1}, converted into MJ m^{-2} per half hour using a multiplier of 0.25 J μmol^{-1}) were made at all sites using LI-COR LI-190 quantum sensors (LI-COR Inc., Lincoln, NE). Incident and reflected PAR sensors were installed on booms at heights of ~28 m and 17 m a.g.l. for OJP-SK and HJP75-SK. Below-canopy incident PAR measurements were made at OJP-SK and HJP75-SK at a height of ~1 m located at the top of the small towers and on level, 1 m booms. At sites in Nova Scotia (NS) incident PAR measurements were made at one location in an open field within 1 km of the forest stands at a height of 2 m and on a level, 1 m extended boom. Reflected above-canopy measurements were not made at the NS sites, therefore, fPAR estimates were incident, rather than absorbed. For consistency, ρ_a was not included in the calculation of fPAR at Nova Scotia sites using HP. None of the sites examined measured below-canopy reflected PAR from the ground surface (e.g. Gower et al., 1999). Measurements were made over 30-minute average periods at each site for most days since 1999 (OJP-SK) and 2004 (HJP75-SK), but were examined from June 1st to September 30th, 2005 at BERMS sites. PAR measurements were made for one week between September 15 and 20, 2007 at 15-minute intervals at NS sites. These included one diffuse radiation day and four direct radiation days. Longer time series of PAR data exist at the NS sites, from September through to November 2007, but these were planned to capture changes in senescence, rather than full growing season fPAR. Low solar zenith angle influences will slightly increase measured fPAR values at the Annapolis Valley sites (Gower et al., 1999). PAR sensors in NS were also calibrated to open-sky PAR for one week prior to analysis.

Diffuse PAR (Model BF3, Delta-T Inc. Cambridge, UK) was also measured during the 2005 growing season at OJP-SK at a height of 28 m to determine the ratio of diffuse to direct PAR days applied to all BERMS jack pine sites (located within 6 km of each other). Daily fPAR and diffuse vs. direct PAR conditions were examined at 12:00 local time on the day that HP was collected for direct comparison between fPAR estimation methods, and also, to avoid the influence of diurnal solar zenith angles.

3.3. Lidar data collection and processing

Lidar data were collected at each site using two generations of Optech, Inc. (Toronto, Canada) Airborne Laser Terrain Mappers

(ALTMs). Data collections prior to 2005 were planned, collected and processed by Optech Inc. All lidar data collections from 2005 to 2007 were organized, collected, and processed by the authors using the Applied Geomatics Research Group (AGRG) ALTM 3100. Table 3 provides details of the lidar data collections and survey parameters used. All sites except for Wolf Creek and Scotty Creek were flown with 50% overlap of scan lines. This ensured that objects on the ground and visible to the receiving optics were viewed from two directions.

Laser pulse ranges, aircraft movement (pitch, roll and heading), and ground and airborne GPS trajectories were combined within the REALM (Optech Inc. Toronto, Ontario) and POSPAC (Applanix Inc., Toronto, Ontario) proprietary software processing packages at the AGRG. POSPAC was used initially to extract positional GPS and attitude information from an inertial measurement unit and position orientation system within the laser head to create a forward and reverse trajectory of aircraft position. This information was then combined in REALM with the laser timing information to create an x, y, z coordinate of laser reflection at the point where the laser pulse intercepts a feature on, or near the ground surface.

After the initial processing of lidar range files and GPS, x, y, z, and intensity files were imported into the software package Terrascan (Terrasolid, Finland) for classification and subsetting of lidar data traps. Each larger area dataset was first filtered for outlying (far above and below ground) laser returns and then classified into laser returns from the ground surface ("ground"). All returns, including those from the ground were kept in a separate "all" file (P_{all} (2)). Ground classification was required to provide a DEM from which P_{all} return datasets can be normalized relative to the ground. Therefore, instead of ellipsoid-based z heights, these were normalized to approximate vegetation heights up to 30 m. This allows for the division of returns into canopy, P_{canopy} (above 1.3 m (or 0.7 m in the case of HJP94)) and remaining (P_{all}) returns required by Eq. (2). GPS plot coordinates were then applied on a per photo plot basis for the extraction of all laser pulse returns within a circular 11.3 m radius to reduce the influence of geo-location errors and to account for the field of view of HP. Normalization of P_{all} data trap returns was performed from "ground" returns using Golden Software Inc. Surfer (Golden, CO) with an inverse-distance weighting procedure of 2 m resolution. Return counts were determined on a 1 m×1 m×height (m) column throughout the canopy to determine fractional canopy cover based on Eq. (3) and calibrated using HP for spatial mapping of fPAR throughout the White Gull River watershed at BERMS. The return density of laser pulses within the White Gull River watershed dataset was approximately eight returns per m^2.

3.4. MODIS data

The MODIS fPAR product (MOD15A2 Collection 4.0) on board the Terra platform, was obtained for the lower part of the White Gull River watershed during composited 8-day periods (www.modis.ornl.gov/modis/index.cfm). Collection 4.0 was used because, at the time of analysis, Collection 5.0 fPAR/LAI products were not yet available. MODIS fPAR products have a few problems associated with them. These include: a) artificial fPAR variability when snow is found within pixels (e.g. Turner et al., 2006); b) poor frequency of data retrievals due to atmospheric contamination (e.g. Coops et al., 2007); c) inability to classify deciduous and evergreen forests within the eight-class biome map; and d) overestimation of LAI due to saturation in dense vegetation (http://landweb.nascom.nasa.gov/). MODIS fPAR pixels from the watershed were retrieved and examined during four composited periods: July 12, 2005; July 28, 2005; August 5, 2005; and August 29, 2005. These days were chosen because a) fPAR did not vary greatly on a per pixel basis between days (less than 15%), when pixels met the highest quality control indices that accompany the MOD15A2 product; and b) MODIS fPAR centered on the approximate time of the lidar survey (August 12, 2005). Optical estimates of fPAR also varied by less than 5% over the growing season at these sites (Chen, 1996). This indicates that accurate fPAR estimates at a single "snap-shot" in time may be adequate for MODIS fPAR product assessment during unchanging canopy conditions, but may not be as useful during shoulder periods or during times when atmospheric constituents, illumination angles, and changing vegetation and ground characteristics alter spectral reflectance. Pixels within the watershed that did meet the highest quality control standards on these days were averaged on a per pixel basis so as to minimize any further discrepancies in the dataset due to seasonal phenology, illumination conditions, or any other slight variations in fPAR.

MODIS pixels were reprojected from the native Integerized Sinusoidal Projection (ISIN) to local Universal Transverse Mercator (UTM) coordinates for comparison with lidar based on four corner coordinates within the 7 km×18 km watershed and a central coordinate. This resulted in a shifting of pixels throughout the watershed, but did not account for the reprojection of parallelogram shaped pixels (MODIS) to square pixels (lidar). Turner et al. (2004a,b) note that reprojection from ISIN to UTM can lead to potentially large errors in pixel geo-location at high latitudes, but have not stated the range of possible errors. Seong et al. (2002) also evaluated reprojection errors from ISIN to UTM and vice versa with latitude and found that the minimum reprojection accuracy from ISIN to UTM (highest

Table 3
Lidar survey configurations and dates per large area site

Survey site location	Date(s) of survey	Lidar model used (Optech Inc. Models)	Flying height (m a.g.l)	Pulse repetition frequency (kHz)	Scan angle (degrees)	Approx. resolution (between returns)	Type and number of returns
York Regional Forest, ON	July 29, 2002	ALTM 2050	850	50	±12	0.9	First, last (2)
	July 9, 2007	ALTM 3100	1000	70	±18	0.9	First, intermediate, last (3)
Bow Summit, AB	Aug. 22, 2002	ALTM 2050	1000	50	±18	1.0	First, last (2)
Lake Utikama, AB	Aug. 30, 2002	ALTM 2050	1200	50	±16	1.0	First, last (2)
BERMS, SK	Aug. 12, 2005	ALTM 3100	950	70	±19	0.50	First, intermediate, last (4)
Annapolis Valley, NS	March 6, 2006	ALTM 3100	1200	70	±20	0.8	First, intermediate, last (4)
	May 13, 2006	ALTM 3100	1000	70	±20	0.8	First, intermediate, last (4)
	May 26, 2006	ALTM 3100	1000	70	±20	0.8	First, intermediate, last (4)
	Aug. 9, 2006	ALTM 3100	1000	70	±20	0.8	First, intermediate, last (4)
	Oct. 5, 2006	ALTM 3100	1000	70	±20	0.8	First, intermediate, last (4)
	July 18, 2007	ALTM 3100	1000	70	±20	0.8	First, intermediate, last (4)
	Aug. 20, 2007	ALTM 3100	1000	70	±20	0.8	First, intermediate, last (4)
	Oct. 1, 2007	ALTM 3100	1000	70	±20	0.8	First, intermediate, last (4)
	Nov. 26, 2007	ALTM 3100	1000	70	±20	0.8	First, intermediate, last (4)
Lac Duparquet, QC	July 11, 2007	ALTM 3100	600	50	±10	0.5	First, intermediate, last (4)
Wolf Creek, YT	August 11, 2007	ALTM 3100	1350	33	±23	1.0	First, last (2)
Scotty Creek, NWT	August 15, 2007	ALTM 3100	550	33	±25	1.5	First, last (2)
Baker Creek, NWT	August 22, 2007	ALTM 3100	1200	70	±25	0.5	First, intermediate, last (4)

Table 4
Comparisons between 2005 average L_e and fPAR estimates using TRAC and LI-2000 along transects at OJP-SK, HJP75-SK, and HJP94-SK within the BERMS study area (Chen et al., 2006) and HP estimates of L_e from this study (columns 2, 3, and 4)

Site	Average plot L_e (HP)	Maximum (HP)	Minimum (HP)	Transect L_e TRAC (m^2 m^{-2})	Transect L_e LI-2000 (m^2 m^{-2})	Transect green fPAR at noon Aug. 15, 2005
	(m^2 m^{-2})	(m^2 m^{-2})	(m^2 m^{-2})	(Chen et al.)	(Chen et al.)	(Chen et al.)
OJP	1.51	1.82	1.21	1.76	1.68	0.49
HJP75	1.74	2.32	1.26	1.86	2.07	0.54
HJP94	0.36	0.83	0.16	0.48	–	0.22

latitudes) was 90.5%, whereas the maximum accuracy (lowest latitudes) was 100%, with a mean accuracy of 98.4%. The accuracy of reprojection from UTM to ISIN was between 98.5% and 99.9%, and is more appropriate than converting from ISIN to UTM. In this study, fPAR estimated from lidar ($fPAR_{lidar}$) was determined at 1 m resolution and then averaged within individual MODIS pixels and subtracted from MODIS fPAR ($fPAR_{MODIS}$) pixels. It is likely that reprojection from ISIN to UTM has introduced some error due to the co-location of MODIS and lidar ~1 km^2 pixels, but when comparing with average $fPAR_{lidar}$, reprojection likely has minimal effect.

4. Results and discussion

4.1. Validating fPAR from HP using radiation sensors

Comparisons between site averages using transect data presented in Chen et al. (2006) and HP used in this study at OJP-SK, HJP75-SK, and HJP94-SK sites are shown in Table 4. In this study, we find that despite differences in the locations of HP plots and transects in Chen et al. (2006), L_e estimates were slightly lower than estimates made using TRAC and LI-2000 methods, but were within 15% at the fairly homogeneous OJP and HJP75 sites and 25% within the heterogeneous HJP94 site. It is likely that average HP L_e methods varied slightly from estimates of Chen et al. (2006) due to variability in canopy cover and an inability to directly locate and compare measurements.

When examining the differences between fPAR estimates made from PAR sensors during diffuse and direct radiation conditions (1200 LST) at OJP and HJP75 (Fig. 3), we find that fPAR was greater and more variable during direct (sunny) days at OJP and HJP75 than during diffuse days, on average (Gower et al., 1999). This variability was primarily due to sun flecks within the canopy.

When comparing between radiation sensors and HP methods (rings 1–9) (Table 5), fPAR estimated using HP methods were lower than fPAR estimated at OJP and HJP75, but closely approximates the fraction of PAR intercepted by the canopy (FIPAR) at sites in Nova Scotia (NS) (MAMW, IB, and MHW). The use of rings 1–9 more closely approximates PAR sensor fPAR than rings 1–5 because of inclusion of more of the lower part of the canopy (comparable to PAR measurements). Differences in fPAR estimated using PAR sensors and HP at OJP and HJP75 were likely because the HP did not view the same canopy as PAR sensors (baselines were up to 100 m and 500 m from PAR sensors). However, at the NS sites, HP and PAR sensor estimates of fPAR were made within 1 m of each other. These results suggest that HP is representative of radiation sensors when HP and PAR measurements are made within close proximity of each other, although more sites should be included for a more thorough analysis.

4.2. Relationship between fPAR from HP and lidar fractional canopy cover

The positive relationship between lidar fractional canopy cover (*f*cover) estimated from Eq. (2) and HP fPAR from annulus rings 1 to 5 is clearly visible for most sites, vegetation species types, ages, phenological structure characteristics, and varying lidar survey configurations in Fig. 4. Table 6 provides average HP fPAR and lidar *f*cover estimates per species type, as well as inputs into the HP fPAR model. Correlation coefficient of the relationships between HP fPAR using annulus rings 1 to 9 and lidar *f*cover is 0.67 (RMSE=0.11) (not shown), whereas estimation of fPAR from rings 1 to 2 has a lower correlation coefficient with *f*cover of 0.61 (RMSE=0.13) (not shown). An analysis of site and species-specific averages ($n=37$) has a similar slope of 0.91, and a coefficient of determination (r^2) of 0.74 (not shown). *f*cover tends to estimate higher levels of fPAR when compared to HP methods (~10% on average), possibly due to lidar survey settings (e.g. Hopkinson & Chasmer, in review) bringing the estimates closer to fPAR estimated from radiation sensors and TRAC and LI-2000 estimates of Chen et al. (2006). The relatively small RMSE of 11%

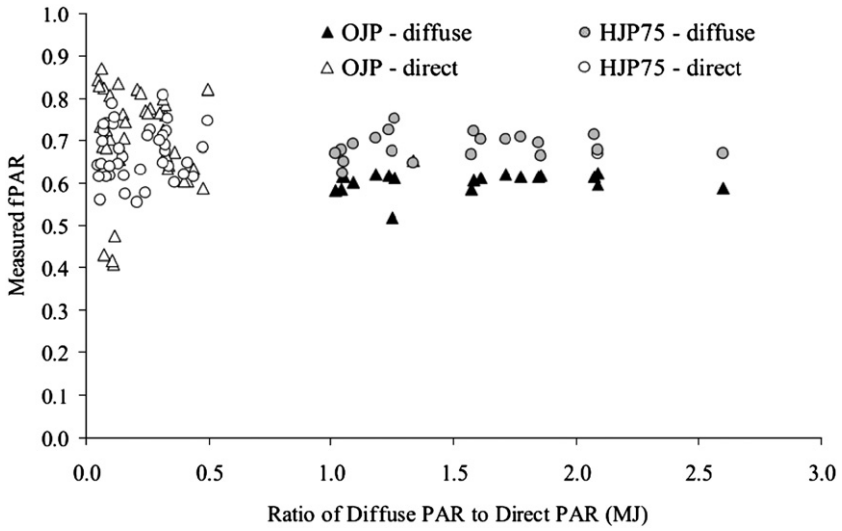

Fig. 3. Comparison of fPAR at 1200 (LST) during midday periods with high and low ratios of diffuse to direct PAR from May 1st to August 31st, 2005 at BERMS (Saskatchewan) jack pine sites.

Table 5
Evaluation of fPAR from HP using PAR sensors at five sites (woody components were included in HP and radiation sensor estimates of fPAR) at noon on the day that the HP was taken

Site	PAR estimated fPAR (diffuse at noon)	PAR estimated PAR (direct at noon)	fPAR from HP (rings 1–5)	fPAR from HP (rings 1–9)	Average *f*cover from Lidar
OJP-SK	0.61	0.70	0.41	0.49	0.46
HJP75-SK	0.69	0.67	0.47	0.51	0.47
MAMW-NS	0.91	0.96	0.88	0.93	0.86
IB-NS	0.90	0.94	0.84	0.90	0.62
MHW-NS	0.89	0.92	0.81	0.86	0.77

Comparisons were also made with lidar fractional canopy cover.

and a coefficient of determination (r^2) of 0.72 implies that this method could be used within canopies of low to moderate LAI (LAI<4.5) examined in this study. Further testing is required for canopies with higher LAI (e.g. >4.5).

When examining differences between *f*cover and HP fPAR for individual species (Table 6), the largest differences occur at sites that a) have not been accurately geo-located (e.g. those plots that were located using handheld GPS or tape measure and bearing methods); and b) have low gap fraction (e.g. Hopkinson & Chasmer, in review). It is expected that *f*cover should be highly correlated with HP fPAR, because L_e used to determine fPAR is estimated directly from canopy Ω (1-fractional cover) and extinction coefficient (k), where $L_e = -\ln(\Omega)/k$. When plot-level HP fPAR and lidar *f*cover were within 10%, plots were accurately located using survey-grade GPS, and also had relatively high fractional canopy cover. Therefore accurate geo-location of plots is very important for registering airborne lidar to HP (Hopkinson & Chasmer, in review; Morsdorf et al., 2006).

Differences greater than 30% between HP fPAR and lidar *f*cover were found in plots that have open canopies and relatively sparse leaf area (e.g. black spruce (BS), white spruce (WS) and sub-alpine fir (SAF)). Coefficients of determination (r^2) between lidar *f*cover and fPAR estimated from HP for BS, WS, and SAF were 0.48, 0.34, and 0.36, respectively using annulus rings 1–5. Regression line slope comparisons (origin=zero) between HP fPAR and *f*cover indicates that lidar fPAR is greater than HP fPAR (slope) by 67% (SAF), 27% (BS), and 21% (WS) (rings 1–5) when compared with the all species average slope. Percent differences in the slope of regression lines were reduced to 54% (SAF), 17% (BS), and 12% (WS) when annulus rings 1–9 were included. This indicates that, for open canopies with branches extending to the ground surface, comparisons with HP rings 1–9 and lidar *f*cover were more appropriate than rings 1–5 in open canopies. Needle-covered branches within BS and SAF stands often extend to the ground surface, but were not captured within HP photographs taken at a height of 1.3 m above the ground, especially using rings 1–5. Rings 1–5 quantify foliage cover directly above the camera, but not at the horizon. Rings 1–9 capture more biomass, but still are unable to measure foliage below the height of the camera within surrounding trees. Airborne lidar does record returns from below the threshold used to define canopy returns (P_{canopy}=1.3 m) but will not record a second return from the ground surface. For returns below ~1.5 m, this indicates an *f*cover of 100%. The return ratio method therefore estimates higher fractional canopy cover than HP at these sites; however, using a lower P_{canopy} threshold would be more realistic of the actual *f*cover than HP estimates. Smaller differences of 17% and 1% (for rings 1 to 5 and 1 to 9) at HJP94-SK, were due to the lower acquisition height of the photograph and lower P_{canopy} thresholds of 0.7 m above the ground. This indicates that adjusting the height of the base of the canopy from lidar improves *f*cover estimates within open canopies.

Sites that have higher fractional canopy cover and less sky-view when compared with other sites (e.g. jack pine (JP), trembling aspen (TA), red pine (RP), Acadian mixed-wood (AMW), hardwood (H), and mature and immature birch (MB, IB)) had correlations (r^2) ranging between 0.53 and 0.66 when fPAR was compared with *f*cover. Line slopes at these sites more closely approximated the average total species line slope of 0.88, and ranged from 0.62 to 0.91. fPAR and *f*cover relationships at these sites were within 12% of the species-based average. AMW and H sites were slightly lower when using lidar *f*cover, and best approximate HP fPAR, whereas the remaining sites (JP, TA, RP, MB and IB) had estimates of HP fPAR that were up to 10% greater. Mixtures of TA and BS had canopy characteristics that were in-between the open conifer sites and more closed canopy sites. Coefficient of determination (r^2) for these sites was 0.32, and the slope of the line (origin=zero) was 0.73. Hopkinson and Chasmer (in review) found that a Beer's Law modified method using laser pulse intensity provided similar results when examining gap fraction, but did not require calibration, unlike results found in this study. Methods discussed in Hopkinson and Chasmer (in review) require geometrically corrected return intensity, which may or may not be available in existing lidar datasets. This study indicates that the return ratio method, without the complex procedures required to geometrically correct return intensity, provides a good approximation of fPAR that can be used to assess the MODIS fPAR product over local to regional areas. Further refinements to fPAR may wish to include geometrically

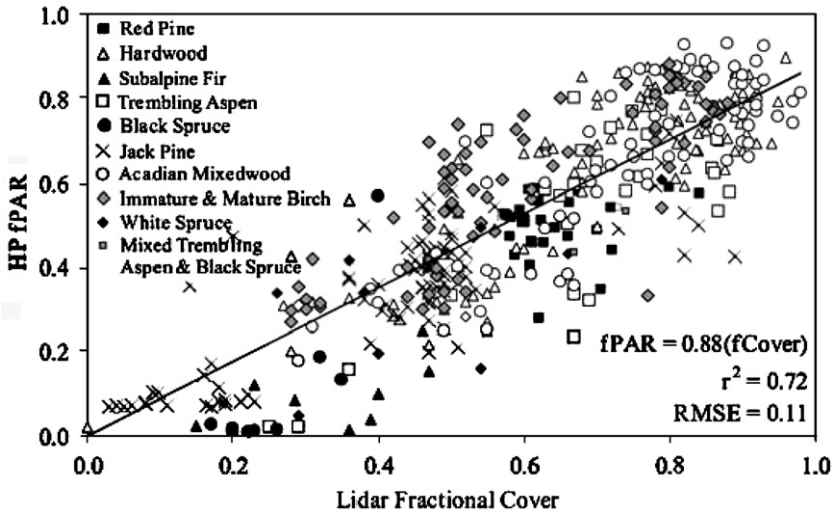

Fig. 4. Comparison between HP fPAR (rings 1–5) and airborne lidar fractional canopy cover (*f*cover) for individual species studied.

Table 6
Average L_e, gap fraction (Ω), fPAR inputs (above-canopy PAR albedo, p_a and below-canopy PAR albedo, p_u) at 12:00 on the day of the photo, and comparisons with average lidar *f*cover

Site code and multiple dates	Ave. L_e (HP)	Ave. Ω (HP)	p_a	p_u	Woody to total leaf area ratio	Ave. *f*cover from lidar	Ave. fPAR from HP rings 1–5 without (and with) p_u and p_a	Ave. fPAR from HP rings 1–9 without (and with) p_u and p_a	Ave. percent difference *f*cover–fPAR (rings 1–5) (no p_u and p_a)	Ave. percent difference *f*cover–fPAR (rings 1–9) (no p_u and p_a)
MRP-ON	1.66	0.42	0.05	0.06	0.07	0.63	0.57 (0.55)	0.50 (0.48)	0.09	0.20
MHW-ON	2.93	0.23	0.03	0.05	0.11	0.88	0.75 (0.73)	0.67 (0.66)	0.15	0.24
MSAF-AB	0.16	0.92	0.05	0.06	0.12	0.35	0.07 (0.07)	0.10 (0.10)	***0.81***	***0.71***
MTA-AB	1.34	0.52	0.03	0.05	0.15	0.70	0.53 (0.52)	0.46 (0.46)	**0.24**	**0.34**
MBS-AB	0.65	0.75	0.05	0.06	0.21	0.52	0.30 (0.29)	0.30 (0.29)	***0.42***	***0.43***
OJP-SK	1.51	0.60	0.05	0.06	0.20	0.46	0.41 (0.40)	0.49 (0.47)	0.11	−0.06
HJP75-SK	1.74	0.62	0.05	0.06	0.15	0.47	0.47 (0.45)	0.51 (0.49)	0.13	−0.08
HJP94-SK	0.36	0.83	0.08	0.15	0.03	0.23	0.19 (0.23)	0.23 (0.26)	0.17	0.01
MTA-QC	2.00	0.34	0.03	0.05	0.21	0.87	0.63 (0.61)	0.58 (0.57)	**0.28**	**0.33**
MB-QC	1.93	0.39	0.03	0.06	0.21	0.78	0.59 (0.59)	0.55 (0.54)	**0.24**	**0.30**
MJP-QC	2.01	0.36	0.05	0.06	0.20	0.81	0.59 (0.56)	0.55 (0.53)	**0.27**	**0.32**
MWS-YT	0.62	0.73	0.05	0.06	0.12	0.49	0.34 (0.33)	0.37 (0.37)	**0.30**	**0.23**
MABS-NWT	1.16	0.53	0.04	0.06	0.15	0.65	0.49 (0.48)	0.45 (0.44)	**0.24**	**0.32**
MTA-NWT	0.55	0.80	0.03	0.05	0.21	0.39	0.23 (0.24)	0.22 (0.23)	**0.41**	**0.44**
NBS-NWT	0.16	0.93	0.05	0.06	0.12	0.27	0.08 (0.09)	0.10 (0.11)	***0.69***	***0.61***
MB-NWT	1.95	0.36	0.03	0.05	0.21	0.50	0.70 (0.69)	0.60 (0.60)	**−0.41**	**−0.21**
MAMW-NS										
04/08/2006	1.13	0.55	0.05	0.05	0.11	0.46	0.44 (0.41)	0.42 (0.40)	*0.26*	*0.28*
05/12/2006	1.24	0.58				0.59	0.51 (0.48)	0.50 (0.48)	−0.09	−0.07
05/27/2006	2.35	0.28				0.78	0.71 (0.68)	0.65 (0.62)	0.09	0.17
08/18/2006	3.32	0.17				0.93	0.85 (0.81)	0.79 (0.75)	0.08	0.15
10/08/2006	2.98	0.22				0.78	0.89 (0.85)	0.86 (0.82)	−0.14	−0.10
07/24/2007	3.17	0.19				0.92	0.79 (0.75)	0.71 (0.67)	0.14	0.23
10/24/2007	3.41	0.17				0.86	0.91 (0.86)	0.85 (0.81)	−0.06	0.01
12/24/2007	0.89	0.65				0.68	0.63 (0.60)	0.60 (0.60)	−0.07	0.11
IB-NS										
04/08/2006	0.62	0.71	0.03	0.06	0.21	0.30	0.29 (0.31)	0.31 (0.32)	0.01	−0.04
05/12/2006	0.80	0.65				0.47	0.32 (0.33)	0.31 (0.32)	*0.31*	*0.34*
05/27/2006	2.23	0.31				0.62	0.64 (0.63)	0.58 (0.57)	−0.03	0.07
08/18/2006	3.19	0.18				0.81	0.81 (0.79)	0.73 (0.72)	0.01	0.10
10/08/2006	1.13	0.54				0.53	0.54 (0.54)	0.49 (0.49)	−0.02	0.07
07/24/2007	3.32	0.17				0.82	0.76 (0.75)	0.68 (0.67)	0.07	0.17
10/24/2007	2.99	0.21				0.62	0.84 (0.82)	0.77 (0.77)	*−0.35*	*−0.23*
12/24/2007	0.68	0.69				0.50	0.54 (0.54)	0.48 (0.48)	−0.09	0.02
MHW-NS										
04/08/2006	0.68	0.70	0.05	0.05	0.11	0.35	0.34 (0.35)	0.35 (0.37)	0.02	−.0.06
05/12/2006	0.77	0.66				0.52	0.34 (0.35)	0.37 (0.35)	*0.34*	*0.33*
05/27/2006	1.95	0.36				0.66	0.64 (0.63)	0.60 (0.59)	0.02	0.08
08/18/2006	3.01	0.20				0.84	0.82 (0.80)	0.76 (0.74)	0.02	0.09
10/08/2006	2.36	0.30				0.71	0.81 (0.79)	0.77 (0.76)	−0.15	−0.10
07/24/2007	3.13	0.20				0.82	0.77 (0.76)	0.70 (0.68)	0.06	0.15
10/24/2007	2.55	0.26				0.77	0.83 (0.81)	0.77 (0.75)	−0.08	0.00
12/24/2007	0.67	0.22				0.55	0.53 (0.53)	0.54 (0.54)	0.03	0.03

Larger percent differences between *f*cover and HP fPAR due to geo-location issues are shown in bold. Low fractional canopy cover due to species type of phenological stage are shown in italics. Negative differences indicate that HP fPAR was greater than lidar *f*cover.
Woody to total ratios from Gower et al. (1999) and Chen et al. (1997). Albedo estimates above and below canopy from Liang et al. (2006), Zhou et al. (2003), and Chen (1996).

corrected return intensity, as suggested in Hopkinson and Chasmer (in review) and variable P_{canopy} height thresholds based on canopy openness.

4.3. Using lidar to assess MODIS fPAR within a medium-sized watershed

Apart from the benefits of classifying the spatial variability in fPAR between and within stands, lidar may also be used to assess the accuracy of vegetation products from lower spectral resolution satellites, such as MODIS. MODIS sensors onboard Aqua and Terra satellite platforms provide daily spectral reflectance measurements of the earth's surface at approximate spatial resolutions of 250 m, 500 m, and 1 km (Running et al., 2004). The evaluation of MODIS vegetation products using optical LAI and fPAR methods has been underway since data collection commenced in early 2000 (Terra) and 2002 (Aqua), resulting in a number of improved leaf area products (e.g. Heinsch et al., 2006; Liang et al., 2006; Pisek & Chen, 2007; Turner et al., 2003; Zhao et al., 2005). The validation of MODIS vegetation products, although essential, is often limited in areas of heterogeneous or "patchy" vegetation types. Sampling of dominant and sub-dominant vegetation patches within the landscape requires extensive plot or transect measurements which can be time consuming and expensive to collect, especially if accurate (e.g. survey-grade) GPS measurements are required (Chasmer et al., in review; Fernandes et al., 2004; Heinsch et al., 2006; Turner et al., 2006; Xu et al., 2004). Further, fPAR from MODIS is an integral component of the GPP model used to estimate global vegetation production and CO_2 uptake by the terrestrial biosphere (Heinsch et al., 2003).

We applied the simple return ratio in Eq. (2), adjusted based on the generalized relationship between lidar *f*cover and HP estimates of fPAR for several species and age classes within a medium-sized watershed for comparison with MODIS fPAR. Lidar *f*cover was determined for 1 m × 1 m × height columns throughout the watershed using a P_{canopy} threshold of 1.3 m. The high resolution lidar data was used to produce detailed maps of fPAR for a variety of vegetation types within a section of the White Gull River watershed in Saskatchewan Canada (also containing jack pine sites (OJP-SK, HJP75-SK and HJP94-SK (BERMS)), and surveyed on the same day) (Fig. 5). This watershed also contains two other eddy covariance flux stations operated by the

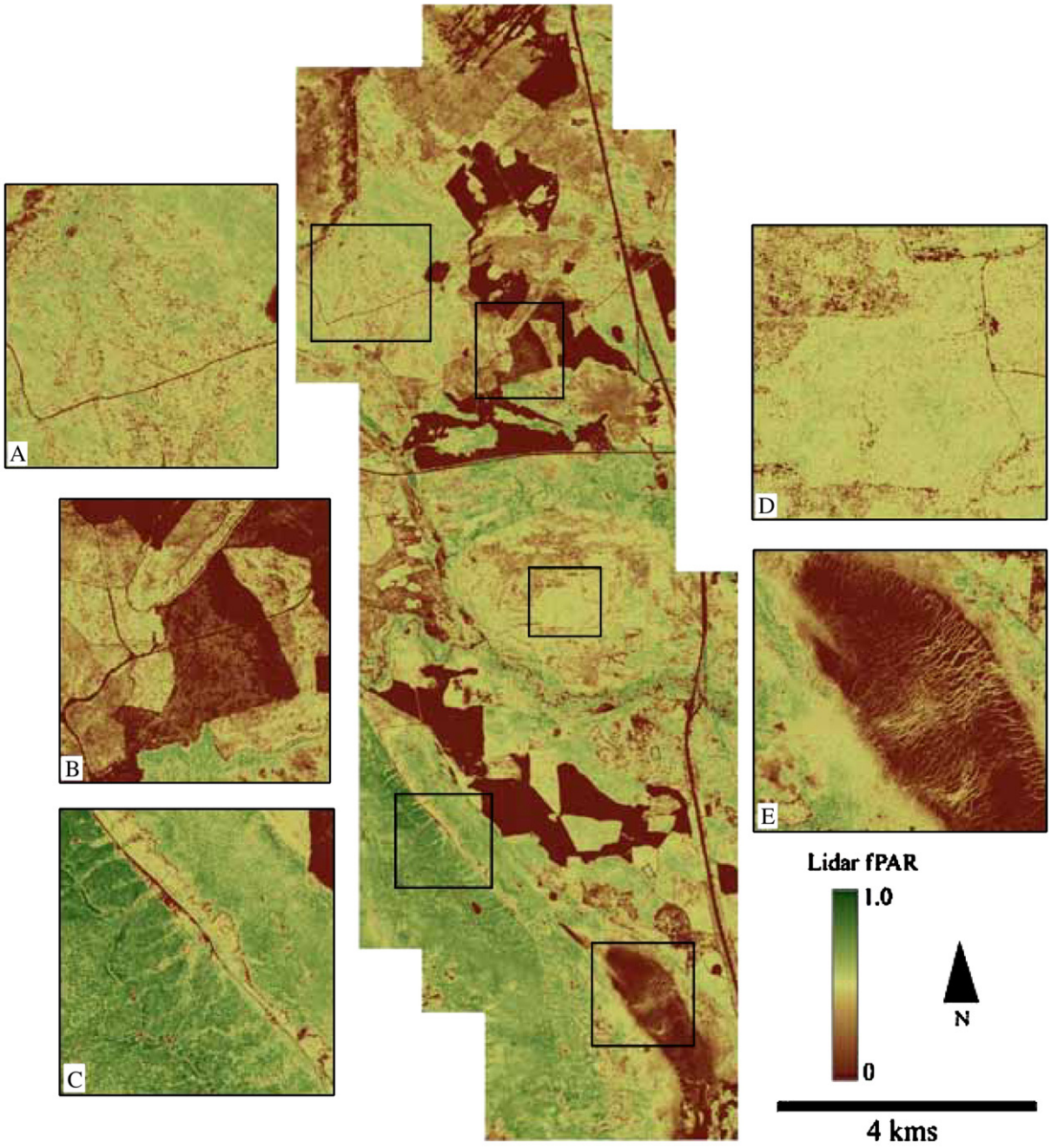

Fig. 5. fPAR estimated from airborne lidar using the ratio of the number of canopy to total returns (2), and the regression model for all species (annulus rings 1–5, used) at a spatial resolution of 1 m. Subset areas have been expanded to show details in the spatial heterogeneity of fPAR. These include A) OJP, B) HJP94, C) riparian zone of the White Gull River, D) HJP75, and E) fen site, also monitored by the Canadian Carbon Program. Recent clear cuts have fPAR values close to zero, whereas low-lying shrub and grass vegetation >1.3 m in height, near the White Gull River, have fPAR values approaching one.

Canadian Carbon Program (not used in this study). The area covered by lidar is up to 7 km wide × 18 km in length, and contains 99 MODIS comparison pixels (~1 km resolution). Five biome types, determined based on the MODIS IGBP classification per pixel were found within the watershed. The biome types include: evergreen needleleaf forest, deciduous broadleaf forest, mixed forest, grassland and permanent wetlands. Subset areas in Fig. 5 illustrate spatial patterns of fPAR within different vegetation types, including patches of recently harvested forests (b), areas of high leaf cover and low-lying vegetation adjacent to the White Gull River (c), and the linear growth of vegetation within a fen (e). The watershed is partly managed and contains a mixture of heterogeneous land cover types typical of the Canadian boreal forest. These are also problematic for MODIS fPAR product accuracy due to the fragmentation of the landscape.

Comparisons between lidar fPAR ($fPAR_{lidar}$) and MODIS fPAR ($fPAR_{MODIS}$) are shown visually for the lower watershed in Fig. 6. $fPAR_{MODIS}$ has been averaged using best quality controlled pixels (>75% of watershed at a time) during four specified periods in July and August 2005 to provide a single estimate of fPAR. Dates included: July 12, 2005; July 28, 2005; August 5, 2005; and August 29, 2005 when fPAR was not changing. $fPAR_{lidar}$ were averaged within each geo-referenced MODIS pixel area and subtracted from $fPAR_{MODIS}$. The difference image has been superimposed as transparent pixels on top of the lidar fPAR map shown in Fig. 5 using the software package ArcGIS 9.2 (ESRI, CA). The purpose of Fig. 6 was to demonstrate differences between lidar and $fPAR_{MODIS}$ across the watershed, and also, to show spatial vegetation heterogeneity within the landscape that might affect the accuracy of $fPAR_{MODIS}$ within some pixels.

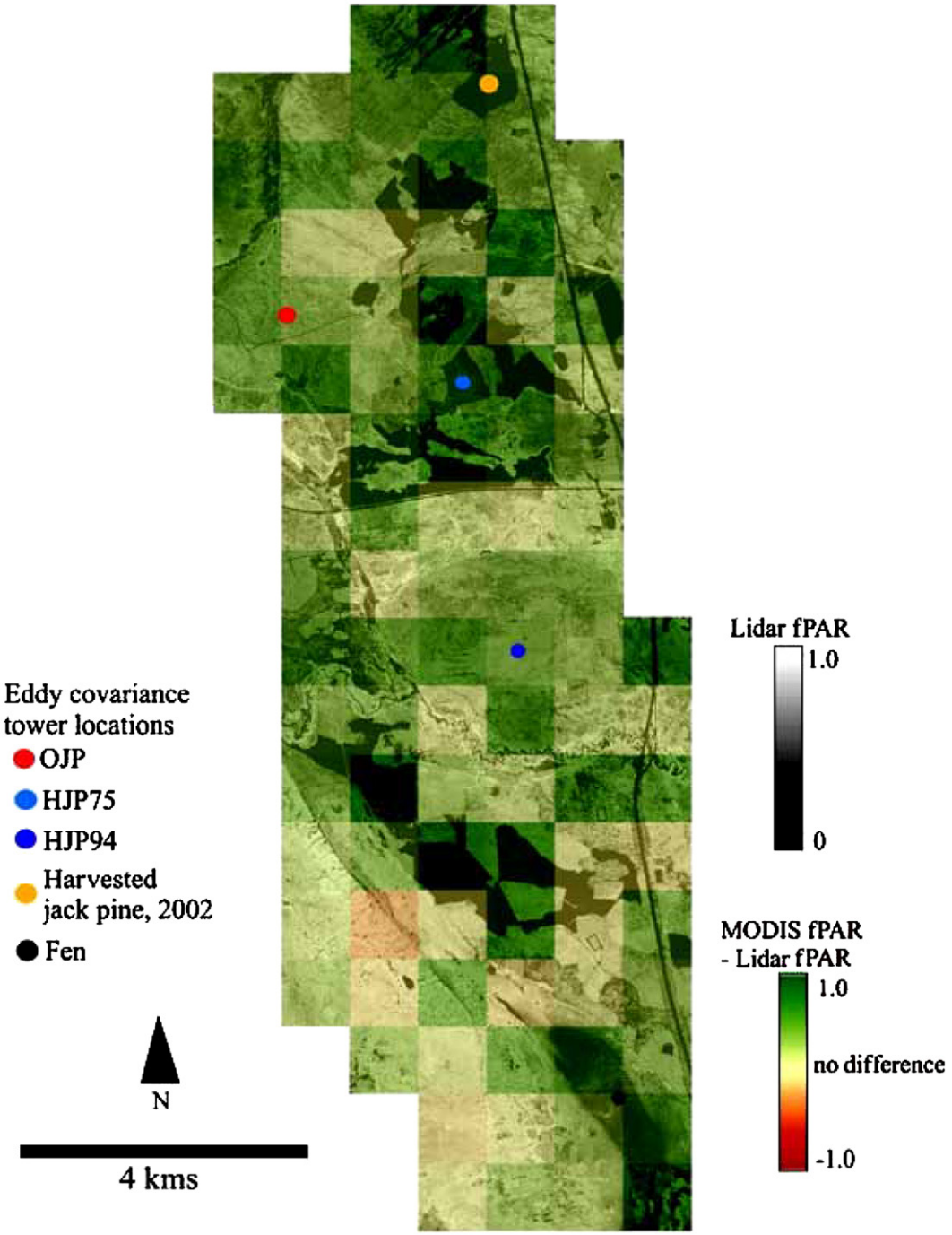

Fig. 6. Two maps are illustrated in this figure. The first map (illustrated in dark to light tones) shows $fPAR_{lidar}$ at 1 m resolution. Overlaid on top of the $fPAR_{lidar}$ map is the difference between average 1 km×1 km $fPAR_{lidar}$ subtracted from $fPAR_{MODIS}$ shown as transparent pixels. Shades of green indicate that $fPAR_{MODIS}$ was greater when compared $fPAR_{lidar}$. Shades of red indicate that $fPAR_{MODIS}$ was lower than $fPAR_{lidar}$.

Average $fPAR_{MODIS}$ for the watershed was 0.73 (stdev.=0.07), whereas average $fPAR_{lidar}$ for the watershed was 0.40 (stdev.=0.24). MODIS pixels that had greater estimates of fPAR when compared with $fPAR_{lidar}$ were those containing recently clear cut areas and a fen. Approximately 22% of pixels within the watershed were in this category. MODIS did provide good estimates of fPAR (within 10% of $fPAR_{lidar}$) within pixels that were relatively homogeneous. These contribute to approximately 24% of the watershed. The remaining pixels were over-estimated by up to 30%, even in some areas where homogeneous pixels exist. Hansen et al. (2000) found that the global vegetation classification scheme is approximately 85% correct. We find that, 21% of pixels were mis-classified as either woody savanna, instead of evergreen needleleaf forest or evergreen needleleaf forest instead of open grassland (determined from 76 handheld GPS point measurements taken within large and homogeneous patches throughout the watershed). Pixels that were evergreen needleleaf, but classified as woody savanna better approximated fPAR from lidar for the same pixels. These results show that the watershed area falls just outside of the average MODIS land classification accuracy.

There are a number of possible reasons for the differences found between some $fPAR_{MODIS}$ pixels and average $fPAR_{lidar}$. These may stem from inaccuracies associated with the lidar approach, or problems within the MODIS fPAR product.

One possible cause of error may be found in $fPAR_{lidar}$. The lidar algorithm (2) does not take into account the fractional cover of grasses and bryophytes because of the inability to separate pulses between short grasses or understory and the ground below ~1.5 m a.g.l. (Hopkinson et al., 2005). Serbin et al. (in press) found that the understory canopy can be a significant part of the total ecosystem fPAR, especially in areas of open canopies. $fPAR_{lidar}$ within grassland and recently cleared patches were close to zero, resulting in apparently large over-estimates by $fPAR_{MODIS}$ when such large differences may not exist. Further, a P_{canopy} threshold height of 1.3 m should be adjusted downwards (to 0.7 m, for example) within open canopies and recently regenerating sites to capture biomass that will likely be observed in MODIS pixels. Classifying areas of open canopies, and lowering the canopy threshold height will reduce differences between lidar and MODIS fPAR.

$fPAR_{MODIS}$ may be greater than fPAR estimated from radiation sensors and HP because usually only the dominant canopy is included in optical measurements (Heinsch et al., 2006; Wang et al., 2004). For example, Heinsch et al. (2006) found that almost one half of LAI observed using MODIS over-estimated site-specific LAI. Wang et al. (2004) and Heinsch et al. (2006) found that MODIS greatly over-estimated fPAR at evergreen needle leaf sites with an open canopy and a significant understory. They suggest that sites with open canopies should consider the understory contribution to fPAR and LAI. We also found that MODIS had higher estimates of fPAR at OJP when compared with $fPAR_{lidar}$. This site has an alder understory located within some parts of the ecosystem that were not included in either the $fPAR_{lidar}$ or HP fPAR estimates. The alder understory will increase $fPAR_{MODIS}$ due to increased foliage cover within pixels. MODIS is similar to lidar because it receives information vertically, from both the canopy and understory, as well as horizontally over the entire pixel (although the light source differs significantly). Lidar may be used to define understory vegetation below the base height of the canopy, but above the ground surface. This assumes that the understory has a fractional cover of 100% (per return resolution, e.g. 1 m) due to the ~1.5 m "blind area" of lidar. This would increase fPAR estimates of lidar relative to MODIS and may provide more comparable estimates of fPAR within a MODIS pixel. Further research should focus on this topic.

Another issue with MODIS fPAR products occurs as a result of the fPAR retrieval algorithm every eight days and during a variety of illumination conditions and solar zenith angles at the time of satellite overpass. Coops et al. (2007) found that only 17% of fPAR retrievals were derived from directionally corrected reflectances (Knyazikhin et al., 1999) over a five year period at a site in British Columbia. The remaining composited periods were determined from NDVI relationships per biome and were often noisy as a result of cloud cover and snow. Further, geo-location issues within composited datasets can reduce the locational accuracy of MODIS pixels by ~10% (or 100 m) in any direction (Wolfe et al., 2002) and conversion from ISIN to UTM will lead to additional co-locational errors of ~3% at the latitude of the White Gull River watershed (Seong et al., 2002). This could affect the differences between $fPAR_{MODIS}$ and $fPAR_{lidar}$, where MODIS reflectance may come from areas beyond the pixel, but are not accounted for by lidar.

5. Conclusions

In this study, a simple ratio of the number of canopy to total returns from airborne lidar was used to estimate fPAR for a number of species types, phenologies, ages, and lidar survey configurations across Canada. The results of this study indicate that airborne lidar canopy fractional canopy cover (*f*cover) can be directly related to fPAR derived from hemispheric photographs (HP), and indirectly related to fPAR derived from PAR sensors above and below plant canopies. Improvements to the *f*cover model and closer association with fPAR from HP may include canopy height (e.g. Riaño et al., 2004; Thomas et al., 2006), or laser pulse intensity (e.g. Hopkinson & Chasmer, 2007, in review). Lidar fPAR was then related to MODIS fPAR across a medium-sized watershed. The results of the analysis show that MODIS typically had higher estimates of fPAR within recently clearcut areas, but was often within 10% of lidar fPAR when examined for homogeneous pixels. These results are important because they demonstrate that MODIS fPAR may be spatially evaluated using lidar. Airborne lidar also provides the ability to assess within-pixel canopy structure, land cover patterns, and fragmentation, as well as the potential impact of understory species. These have been cited as potential issues affecting MODIS land cover products, apart from atmospheric contamination of pixels and meteorological inputs discussed within recent literature. The availability of lidar data will enable further development and research into the methods discussed, including application within sites of greater leaf area and adjustment for understory species.

Acknowledgements

The Applied Geomatics Research Group for access to technology and computer resources, and Optech Inc. for the early lidar surveys; Benoit St Onge, Abitibi Model Forest; the Canadian Carbon Program (CCP) Boreal Ecosystem Research and Monitoring Sites (BERMS); John Pomeroy and William Quinton, Improved Processes for Parameterisation and Prediction in cold regions (IP3); Ron Hall, Canadian Forest Service; and Irena Creed, Hydrology, Ecology and Disturbance of wetland complexes in northern Alberta (HEAD) network for partnership. The Climate Research Division, Atmospheric Sciences and Technology Directorate, Environment Canada for financial support for the lidar survey at BERMS. People who helped with photography and GPS surveys include: Chris Beasy, Bruce Davison, Jordan Erker, Stella Heenan, John Barlow, Ron Chasmer, Rodney Clark, Gabor Sass, Doug Stiff, Kevin Garroway, and Allyson Fox. Allyson Fox is also thanked for processing the IP3 lidar datasets. MODIS data were obtained with thanks from the Oak Ridge National Laboratory Distributed Active Archive Center (ORNL DAAC). 2007 MODIS subset land products are available on-line [http://www.daac.ornl.gov/MODIS/modis.html] from ORNL DAAC, Oak Ridge, Tennessee, U.S.A. Funding for this project has been provided by CFCAS, NSERC, PREA, and the BIOCAP Canada Foundation. Laura has been generously supported by graduate student scholarships from NSERC and OGSST and research assistantships from CRESTech.

References

Barilotti, A., Turco, S., & Alberti, G. (2006). *LAI determination in forestry ecosystems by LiDAR data analysis.*Workshop on 3D Remote Sensing in Forestry : BOKU Vienna 14-15/02/2006.

Chasmer, L., Hopkinson, C., Smith, B., & Treitz, P. (2006). Examining the influence of changing laser pulse repetition frequencies on conifer forest canopy returns. *Photogrammetric Engineering and Remote Sensing*, *17*(12), 1359–1367.

Chasmer, L., Barr, A., Hopkinson, C., McCaughey, H., Treitz, P., Black, A., Shashkov, A. (in review). Scaling and assessment of GPP from MODIS using a combination of airborne lidar and eddy covariance measurements over jack pine forests. *Remote Sensing of Environment.*

Chen, J., Rich, P., Gower, T. S., Norman, J. M., & Plummer, S. (1997). Leaf area index of boreal forests: theory, techniques and measurements. *Journal of Geophysical Research*, *10*, 29,429–29,444.

Chen, J. M. (1996). Canopy architecture and remote sensing of the fraction of photosynthetically active radiation absorbed by boreal conifer forests. *IEEE Transactions on Geoscience and Remote Sensing*, *34*(6), 1353–1368.

Chen, J. M., Chen, X., Ju, W., & Geng, X. (2005). A remote sensing-driven distributed hydrological model: Mapping evapotranspiration in a forested watershed. *Journal of Hydrology*, *305*, 15–39.

Chen, B., Chen, J. M., Mo, G., Yuan, K., Higuchi, K., & Chan, D. (2007). Modeling and scaling coupled energy, water, and carbon fluxes based on remote sensing: An application to Canada's landmass. *Journal of Hydrometeorology*, *8*, 123–143.

Chen, J. M., Govind, A., Sonnentag, O., Zhang, Y., Barr, A., & Amiro, B. (2006). Leaf area index measurements at Fluxnet-Canada forest sites. *Agricultural and Forest Meteorology*, *140*, 257–268.

Chen, J. M., Pavlic, G., Brown, L., Cihlar, J., Leblanc, S., White, H., et al. (2002). Derivation and validation of Canada-wide coarse-resolution leaf area index maps using high-resolution satellite imagery and ground measurements. *Remote Sensing of Environment*, *80*, 165–184.

Chen, X., Vierling, L., Rowell, E., & DeFelice, T. (2004). Using lidar and effective LAI data to evaluate IKONOS and Landsat 7 ETM+ vegetation cover estimates in a ponderosa pine forest. *Remote Sensing of Environment*, *91*, 14–26.

Coops, N. C., Black, T. A., Jassal, R. S., Trofymow, J. A., & Morgenstern, K. (2007). Comparison of MODIS, eddy covariance determined and physiologically modelled gross primary production (GPP) in a Douglas-fir forest stand. *Remote Sensing of Environment*, *107*, 385–401.

Eriksson, H. M., Eklundh, L., Kuusk, A., & Nilson, T. (2006). Impact of understory vegetation on canopy reflectance and remotely sensed LAI estimates. *Remote Sensing of Environment*, *103*, 408–418.

Fernandes, R. A., Miller, J. R., Chen, J. M., & Rubinstein, I. G. (2004). Evaluating image based estimates of leaf area index in Boreal conifer stands over a range of scales using high-resolution CASI imagery. *Remote Sensing of Environment*, *89*, 200–216.

Fluxnet-Canada (2003). *Fluxnet-Canada measurement protocols, Working Draft Version 1.3*.Laval, Quebec: Fluxnet-Canada Network Management Office Available online: http://www.fluxnet-canada.ca

Gamon, J. A., Huemmrich, K. F., Chen, J. M., Fuentes, D., Hall, F. G., Kimball, J. S., et al. (2004). Remote sensing in BOREAS: Lessons learned. *Remote Sensing of Environment*, *89*, 139–162.

Goel, N., & Thompson, R. (2000). A snapshot of canopy reflectance models and a universal model for the radiation regime. *Remote Sensing Reviews*, *18*, 197–225.

Gower, S. T., Kucharik, C. J., & Norman, J. M. (1999). Direct and indirect estimation of leaf area index, f_{APAR}, and net primary production of terrestrial ecosystems. *Remote Sensing of Environment*, *70*, 29–51.

Hansen, M. C., DeFries, R. S., Townshend, K., & Sohlberg, R. (2000). Global land cover classification at 1 km spatial resolution using a classification tree approach. *International Journal of Remote Sensing*, *21*, 1331–1364.

Hayashi, M., Goeller, N., Quinton, W., & Wright, N. (2007). A simple heat-conduction method for simulating the frost-table depth in hydrological models. *Hydrological Processes*, *21*, 2610–2622.

Heinsch, F. A., Reeves, M., Bowker, C. F., Votava, P., Kang, S., Milesi, C., et al. (2003). User's guide, GPP and NPP (MOD17A2/A3), NASA MODIS Land Algorithm, Version 1.2. www.ntsg.umt.edu/modis/MOD17UsersGuide.pdf

Heinsch, F. A., Zhao, M., Running, S., Kimball, J., Nemani, R., Davis, K., et al. (2006). Evaluation of remote sensing based terrestrial productivity from MODIS using regional tower eddy flux network observations. *IEEE Transactions on Geoscience and Remote Sensing*, *44*(7), 1908–1925.

Hopkinson, C., & Chasmer, L. (2007). Using discrete laser pulse return intensity to model canopy transmittance. *The Photogrammetric Journal of Finland*, *20*(2), 16–26.

Hopkinson, C. & Chasmer, L. (in review). Testing a lidar intensity based model of canopy fractional cover across multiple forest ecozones. *Remote Sensing of Environment*.

Hopkinson, C., Chasmer, L., & Hall, R. (2008). Using airborne lidar to examine forest growth. *Remote Sensing of Environment*, *112*(3), 1168–1180.

Hopkinson, C., Chasmer, L., Lim, K., Treitz, P., & Creed, I. (2006). Towards a universal lidar canopy height indicator. *Canadian Journal of Remote Sensing*, *32*(2), 139–152.

Hopkinson, C., Chasmer, L., Sass, G., Creed, I., Sitar, M., Kalbfleisch, W., et al. (2005). Assessing vegetation height and canopy volume in a Boreal wetland complex using airborne scanning LiDAR. *Canadian Journal of Remote Sensing*, *31*(2), 191–206.

Hopkinson, C., Chasmer, L., Young-Pow, C., & Treitz, P. (2004). Assessing forest metrics with a ground-based scanning LiDAR. *Canadian Journal of Forest Research*, *34*, 573–583.

Hopkinson, C., & Demuth, M. (2006). Using airborne lidar to assess the influence of glacier downwasting on water resources in the Canadian Rocky Mountains. *Canadian Journal of Remote Sensing*, *32*(2), 212–222.

Huemmrich, K. F., Black, T. A., Jarvis, P. G., McCaughey, J. H., & Hall, F. G. (1999). High temporal resolution NDVI Phenology from micrometeorological radiation sensors.*Journal of Geophysical Research*, *104*(D22), 27934–27944 (Special BOREAS Issue H, BOREAS in 1999).

Hyer, E., & Goetz, S. (2004). Comparison and sensitivity analysis of instruments and radiometric methods for LAI estimation: Assessments from a boreal forest site. *Agricultural and Forest Meteorology*, *122*, 157–174.

Jin, Z., Tian, Q., Chen, J. M., & Chen, M. (2007). Spatial scaling between leaf area index maps of different resolutions. *Journal of Environmental Management*, *85*, 628–637.

Jonckheere, I., Fleck, S., Nackaerts, K., Muys, B., Coppin, P., Weiss, M., et al. (2004). Review of methods for in situ leaf area index determination Part 1. Theories, sensors and hemispherical photography. *Agricultural and Forest Meteorology*, *121*, 19–35.

Knyazikhin, Y., Glassy, J., Privette, J., Tian, Y., Lotsch, A., Zhang, Y., et al. (1999). *MODIS leaf area index (LAI) and fraction of photosynthetically active radiation absorbed by vegetation (FPAR) product (MOD15) algorithm theoretical basis document.* http://modis.gsfc.nasa.gov/data/atbd/land_atbd.php

Koetz, B., Sun, G., Morsdorf, F., Ranson, K., Kneubuhler, M., Itten, K., et al. (2006). Fusion of imaging spectrometer and LIDAR data over combined radiative transfer models for forest canopy characterization. *Remote Sensing of Environment*, *106*(4), 449–459.

Kotchenova, S., Song, X., Shabanov, N., Potter, C., Knyazikhin, Y., & Myneni, R. (2004). Lidar remote sensing for modeling gross primary production of deciduous forests. *Remote Sensing of Environment*, *92*, 158–172.

Leblanc, S. G., Chen, J. M., Fernandes, R., Deering, D. W., & Conley, A. (2005). Methodology comparison for canopy structure parameters extraction from digital hemispherical photography in boreal forests. *Agricultural and Forest Meteorology*, *129*, 187–207.

Liang, S., Zheng, T., Liu, R., Fang, H., Tsay, S. -C., & Running, S. (2006). Estimation of incident photosynthetically active radiation from Moderate Resolution Imaging Spectroradiometer data. *Journal of Geophysical Research*, *11*, D15208. doi:10.1029/2005JD006730

Lovell, J., Jupp, D., Culvenor, D., & Coops, N. (2003). Using airborne and groundbased ranging lidar to measure canopy structure in Australian forests. *Canadian Journal of Remote Sensing*, *29*(5), 607–622.

Magnussen, S., & Boudewyn, P. (1998). Derivations of stand heights from airborne laser scanner data with canopy-based quantile estimators. *Canadian Journal of Forest Research*, *28*, 1016–1031.

Morsdorf, F., Kotz, B., Meier, E., Itten, K., & Allgower, B. (2006). Estimation of LAI and fractional cover from small footprint airborne laser scanning data based on gap fraction. *Remote Sensing of Environment*, *104*, 50–61.

Myneni, R. B., Nemani, R. R., & Running, S. W. (1997). Algorithm for the estimation of global land cover, LAI and FPAR based on radiative transfer models. *IEEE Transactions in Geoscience and Remote Sensing*, *35*, 1380–1393.

Pielke, R. A., Avissar, R., Raupach, M., Dolman, A., Xeng, Y., & Denning, S. (1998). Interactions between the atmosphere and terrestrial ecosystems. Influence on weather and climate. *Global Change Biology*, *4*, 461–475.

Pisek, J., & Chen, J. M. (2007). Comparison and validation of MODIS and VEGETATION global LAI products over four BigFoot sites in North America. *Remote Sensing of Environment*, *109*, 81–94.

Pomeroy, J. W., Granger, R. J., Hedstrom, N. R., Gray, D. M., Elliott, J., Pietroniro, A., et al. (2005). The process hydrology approach to improving prediction of ungauged basins in Canada. In C. Spence, J. Pomeroy, & A. Pietroniro (Eds.), *Predictions in ungauged basins: Approaches for Canada's cold regions* (pp. 67–100). Canadian Society for Hydrological Sciences, Environment Canada.

Quinton, W. L., Shirazi, T., Carey, S. K., & Pomeroy, J. W. (2005). Soil water storage and active-layer development in a sub-alpine tundra hillslope, southern Yukon Territory, Canada. *Permafrost and Periglacial Processes*, *16*, 369–382.

Riaño, D., Valladares, F., Condés, S., & Chuvieco, E. (2004). Estimation of leaf area index and covered ground from airborne laser scanner (Lidar) in two contrasting forests. *Agricultural and Forest Meteorology*, *124*, 269–275.

Running, S. W., Nemani, R. R., Heinsch, F. A., Zhao, M., Reeves, M. C., & Hashimoto, H. (2004). A continuous satellite-derived measure of global terrestrial primary production. *BioScience*, *54*, 547–560.

Schwalm, C. R., Black, T. A., Amiro, B. D., Arain, M. A., Barr, A. G., Bourque, C. P. -A., et al. (2006). Photosynthetic light use efficiency of three biomes across an east-west continental-scale transect in Canada. *Agricultural and Forest Meteorology*, *140*, 269–286.

Seong, J. C., Mulcahy, K., & Usery, L. (2002). The sinusoidal projection: A new importance in relation to global image data. *Professional Geographer*, *54*(2), 218–225.

Serbin, S. P., Gower, S. T., & Ahl, D. E., (in press). Canopy dynamics and phenology of a boreal black spruce wildfire chronosequence. *Agricultural and Forest Meteorology*.

Solberg, S., Naesset, E., Hanssen, K. H., & Christiansen, E. (2006). Mapping defoliation during a severe insect attack on Scots pine using airborne laser scanning. *Remote Sensing of Environment*, *102*, 364–376.

Sonnentag, O., Talbot, J., Chen, J. M., & Roulet, T. N. (2007). Using direct and indirect measurements of leaf area index to characterize the shrub canopy of an ombrotrophic peatland. *Agricultural and Forest Meteorology*, *144*, 200–212.

St Onge, B., & Vepakomma, U. (2004). Assessing forest gap dynamics and growth using multi-temporal laser-scanner data. *International Archives of Photogrammetry, Remote Sensing and Spatial Information Sciences*, *XXXVI-8/W2*, 173–178.

Sun, G. Q., & Ranson, K. (2000). Modelling lidar returns from forest canopies. *IEEE Transactions on Geoscience and Remote Sensing*, *38*, 2617–2626.

Thomas, V., Finch, D., McCaughey, J. H., Noland, T., Rich, L., & Treitz, P. (2006). Spatial modeling of the fraction of photosynthetically active radiation absorbed by a boreal mixedwood forest using a lidar-hyperspectral approach. *Agricultural and Forest Meteorology*, *140*, 287–307.

Tian, Y., Wang, Y., Zhang, Y., Knyazikhin, Y., Bogaert, J., & Myneni, R. (2002). Radiative transfer based scaling of LAI retrievals from reflectance data of different resolutions. *Remote Sensing of Environment*, *84*, 143–159.

Tian, Y., Woodcock, C., Wang, Y., Privette, J., Shabanov, N., Zhou, L., et al. (2002). Multiscale analysis and validation of the MODIS LAI product 1. Uncertainty assessment. *Remote Sensing of Environment*, *83*, 414–430.

Todd, K. W., Csillag, F., & Atkinson, P. M. (2003). Three-dimensional mapping of light transmittance and foliage distribution using lidar. *Canadian Journal of Remote Sensing*, *29*(5), 544–555.

Turner, D. P., Ollinger, S., & Kimball, J. (2004). Integrating remote sensing and ecosystem process models for landscape- to regional-scale analysis of the carbon cycle. *BioScience*, *54*(6), 573–584.

Turner, D., Ollinger, S., Smith, M. I., Krankina, O., & Gregory, M. (2004). Scaling net primary production to a MODIS footprint in support of earth observing system product validation. *International Journal of Remote Sensing*, *25*(10), 1961–1979.

Turner, D. P., Ritts, W. D., Cohen, W. B., Gower, S. T., Running, S. W., Zhao, M., et al. (2006). Evaluation of MODIS NPP and GPP products across multiple biomes. *Remote Sensing of Environment*, *102*, 282–292.

Turner, D. P., Ritts, W., Cohen, W., Gower, S., Zhao, M., Running, S., et al. (2003). Scaling gross primary production (GPP) over boreal and deciduous forest landscapes in support of MODIS GPP product validation. *Remote Sensing of Environment*, *88*, 256–270.

Wang, Y., Woodcock, C., Buermann, W., Stenberg, P., Voipio, P., Smolander, H., et al. (2004). Evaluation of the MODIS LAI algorithm at a coniferous forest site in Finland. *Remote Sensing of Environment*, *91*, 114–127.

Wolfe, R. E., Nishihama, M., Fleig, A., Kuyper, J., Roy, D., Storey, J., et al. (2002). Achieving sub-pixel geolocation accuracy in support of MODIS land science. *Remote Sensing of Environment*, *83*, 31–49.

Xu, S., Chen, J. M., Fernandes, R., & Cihlar, J. (2004). Effects of subpixel water area fraction on mapping leaf area index and net primary productivity in Canada. *Canadian Journal for Remote Sensing*, *30*, 797–804.

Zhang, Y., Chen, J., & Miller, J. (2005). Determining digital hemispherical photograph exposure for leaf area index estimation. *Agricultural and Forest Meteorology*, *133*, 166–181.

Zhao, M., Heinsch, F. A., Nemani, R. R., & Running, S. (2005). Improvements of the MODIS terrestrial gross and net primary production global data set. *Remote Sensing of Environment*, *95*, 164–176.

Zhou, L., Dickinson, R. E., Tian, Y., Zeng, X., Dai, Y., Yang, Z. -L., et al. (2003). Comparison of seasonal and spatial variations of albedos from Moderate Resolution Imaging Spectroradiometer (MODIS) and Common Land Model. *Journal of Geophysical Research*, *108*, 4488–4688.